ELSEVIER

Journal of Nuclear Materials 317 (2003) 46–53

journal of nuclear materials

www.elsevier.com/locate/jnucmat

Examination of U valence states in the brannerite structure by near-infrared diffuse reflectance and X-ray photoelectron spectroscopies

Kim S. Finnie *, Zhaoming Zhang, Eric R. Vance, Melody L. Carter

Materials and Engineering Science, Australian Nuclear Science and Technology Organisation, Private Mail Bag 1, Menai, NSW 2234, Australia

Received 17 July 2002; accepted 26 November 2002

Abstract

The valence state of uranium doped into a f^0 thorium analog of brannerite (i.e., thorutite) has been examined using near-infrared (NIR) diffuse reflectance (DRS) and X-ray photoelectron (XPS) spectroscopies. NIR transitions of U^{4+}, which are not observed in spectra of brannerite, have been detected in the samples of $U_xTh_{1-x}Ti_2O_6$, and we propose that strong specular reflectance is responsible for the lack of U^{4+} features in UTi_2O_6. Characteristic U^{5+} bands have been identified in samples in which sufficient Ca^{2+} has been added to nominally effect complete oxidation to U^{5+}. XPS results support the assignments of U^{4+} and U^{5+} by DRS. The presence of residual U^{4+} bands in the spectra of the Ca-doped samples is consistent with segregation of Ca^{2+} to the grain boundaries during high temperature sintering.

1. Introduction

The multiphase titanate ceramic, synroc, has been proposed as a suitable matrix for immobilisation of high-level nuclear waste (HLW) due to the capacity to incorporate almost all HLW ions into the comprising phases (mainly zirconolite, perovskite and hollandite), of which naturally occurring examples have demonstrated geological stability [1]. More recently, synroc derivatives have targeted waste actinides, particularly Pu and U [2]. Predictions of possible cation location can, in general, be made on the basis of ionic radii and charge compensation and are of particular interest in the case of actinide species. However, with a wide range of cation sites available, the final oxidation states of the actinide components are uncertain. This is true even when the redox conditions are known accurately, because there are other factors that affect actinide valences, e.g. the availability of appropriate charge compensators and the crystal-field stabilisation energy. Recently, X-ray near edge spectroscopy (XANES) has been used to determine the oxidation state of uranium, neptunium and plutonium in perovskite and zirconolite, by comparing the band edge position with that of a tetravalent reference [3,4]. It would clearly be of interest to be able to derive similar information in a standard laboratory, given the limitation of a solid, polycrystalline sample. Diffuse reflectance (DRS) and X-ray photoelectron (XPS) spectroscopies are useful techniques for studying the speciation of transition metal ions, lanthanides and actinides in the solid phase, particularly as transitions belonging to different valences of the same element in DRS should not overlap to the extent observed in XANES.

The optical spectra of actinide ions have been extensively investigated, as detailed in a report by Carnall and Crosswhite [5]. In comparison with the lanthanides, which are characterised by weak, sharp electronic transitions within the appropriate $4f^n$ configuration, the 5f

* Corresponding author. Tel.: +61-2 9717 3819; fax: +61-2 9543 7179.

E-mail address: ksf@ansto.gov.au (K.S. Finnie).

0022-3115/03/$ - see front matter
doi:10.1016/S0022-3115(03)00004-7

outer electrons of the actinides are less shielded, and thus configuration interaction is more important. Transitions within what remains essentially a $5f^n$ configuration are correspondingly more intense, and show increased dependence on the surrounding environment. Solution spectra of the trivalent and quadrivalent actinide aquo ions from U to Bk have been published [5], and contain intraconfigurational bands with widths of tens to hundreds of cm^{-1}, ranging through the near-infrared to the visible region. Typically, synroc samples and many of the associated minerals such as brannerite, hollandite and zirconolite, are strongly coloured and thus absorbing in the visible range. However, these oxide materials are less likely to be absorbing in the near-infrared (NIR) region, and hence it may be possible to observe lower-lying f–f transitions of dopant actinide species, thus aiding identification of their oxidation states.

Brannerite, nominally UTi_2O_6 (C^3_{2h}), is a minor synroc phase which can only be synthesised in pure form under low oxygen partial pressure. However, partial substitution of U with Ca^{2+} and Gd^{3+} into the actinide site allows the synthesis of doped brannerite in air, as well as argon [6,7]. Initial DRS measurements of brannerite powder showed no evidence of sharp U^{4+} transitions in the NIR, although a band attributed to U^{5+} was observed in Ca-doped samples [6,7]. Several possible explanations for the lack of U^{4+} bands in the spectrum of UTi_2O_6 have been suggested. The first was that no single-ion U^{4+} exists in pure brannerite, due to electron interaction occurring between neighbouring U^{4+} ions [6]. A latter suggestion was that U^{4+} electric dipole single-ion transitions should be forbidden due to a centre of inversion, (U site symmetry C_{2h}) [7]. This centre of inversion is lost on local substitution with Ca^{2+}, thus allowing transitions of the charge-compensating U^{5+} ion. However, the low reflectance of UTi_2O_6 throughout the NIR suggests that the material does absorb strongly in this region, implying active transitions of the U^{4+} ion, although specific U bands are not observed.

A more likely explanation of the lack of U^{4+} DRS bands in the spectrum of brannerite, is that most of the incident light is specularly reflected by the sample, as predicted for strongly absorbing materials [8]. The contribution of both specular and diffuse reflection to the total reflectance, and the influence of particle size, has been previously reported [9]. Briefly, while we may expect diffuse reflectance to dominate in the case of relatively small grains ($d \sim \lambda$, 1–2 μm), in the case of strong absorption bands, increased specular reflectance can result in a decrease in spectral contrast and apparent 'wash-out' of intense features in a diffuse reflectance spectrum [9]. To test this, we have measured the diffuse reflectance of U^{4+} diluted in thorutite, $ThTi_2O_6$, which has the brannerite structure. Although there are many experimental difficulties in obtaining quantitative data using diffuse reflectance measurements [8], many of these problems can be minimised by diluting the material in a non-absorbing host. A series of compounds with varying U^{4+} content have been analysed, along with corresponding Ca-doped samples nominally containing sufficient Ca^{2+} so that the lattice is charge-compensated by conversion of all the U^{4+} to U^{5+}. In this way, the ambient temperature NIR spectra of the quadrivalent and pentavalent states of U in the thorutite structure have been characterised. The replacement of U with Th is expected to have negligible effect on the U ligand field, and thus observed U band positions are assumed to be characteristic of brannerite. The spectrum of U in perovskite, $Ca_{0.97}U_{0.03}Ti_{0.94}Al_{0.06}O_3$, in which U^{4+} lacks a centre of inversion, is discussed for comparison.

Because XPS has the ability to discriminate between different oxidation states and chemical environments, it has been used widely since the 1970s to determine the surface oxidation state of U in many uranium compounds [10]. The binding energy of the U $4f_{7/2}$ peak is directly related to the oxidation state of uranium. As the oxidation state of uranium increased from U^{4+} (UO_2) to U^{6+} (UO_3), the binding energy of the U $4f_{7/2}$ peak was observed to increase by 1.7–1.8 eV [11,12]. Although only U^{4+} and U^{6+} exist in binary uranium oxides (U_2O_5 contains a mix of U 4+ and 6+ valence states, $U^{4+}U^{6+}O_5$ [10]), the presence of U^{5+} was reported previously in alkali and alkaline earth uranates [13] and doped brannerites [7]. In addition, the shake-up satellite structure associated with the U 4f levels is also very sensitive to its local chemical environment [10]. Although XPS is a surface technique with a probing depth of approximately 5 nm, valuable information regarding the oxidation states in the bulk can still be obtained as long as the sample surface is relatively stable towards atmospheric oxidation. In the current study, only slight surface oxidation was observed in all the U/Ca-doped thorutite samples, therefore XPS has been used along with DRS to determine the U-valency in the brannerite structure.

2. Experimental

2.1. Materials

For the DRS measurements, three U loadings in thorutite were primarily used; (1) $Th_{0.97}U_{0.03}Ti_2O_6$ (U1) and $Th_{0.955}U_{0.03}Ca_{0.015}Ti_2O_6$ (UCa1), (2) $Th_{0.9}U_{0.1}Ti_2O_6$ (U2) and $Th_{0.85}U_{0.1}Ca_{0.05}Ti_2O_6$ (UCa2), and (3) $Th_{0.7}U_{0.3}Ti_2O_6$ (U3) and $Th_{0.55}U_{0.3}Ca_{0.15}Ti_2O_6$ (UCa3). The U series nominally contained only U^{4+}, and the UCa series nominally only U^{5+}. Four samples, U3, UCa3, UCa2 and UCa1, were also examined by XPS. Samples were made by the alkoxide/nitrate route [1] in

which aqueous solutions of Th, uranyl and Ca nitrates were first mixed with stoichiometric amounts of Ti isopropoxide, stir-dried, calcined for 1 h at 750 °C, and wet-milled. The powders were then pelletised and sintered for 20 h at 1500 °C in argon, or air in the case of the Ca^{2+} containing samples. The surfaces used in the DRS and XPS studies were formed by cutting and polishing (or fracturing) after high temperature sintering, and thus are representative of the bulk, aside from slight surface oxidation due to the exposure to air (see below). Polished (0.25 μm) surfaces were carbon coated and characterised by SEM, using a JEOL 6400 instrument operated at 15 keV, and fitted with a Tracor Northern Voyager IV X-ray microanalysis system (EDS). A comprehensive set of standards was used for quantitative work, giving a high degree of accuracy. This verified the compositions and showed the samples to be almost fully reacted. Minor impurity phases (<1%) of rutile and ThO_2 were observed. The composition of the perovskite sample discussed in the text and Fig. 7 is $Ca_{0.97}U_{0.03}Ti_{0.94}Al_{0.06}O_3$, ($Al^{3+}$ added to charge compensate U^{4+} substituted for Ca^{2+}) and was prepared using the method described above.

Flat surfaces for DRS measurements were prepared by polishing with 1200 grit SiC and ethanol. The physical appearance of all of the thorutite samples was very similar, being of a dark grey colour. In order to determine the degree of atmospheric oxidation at the surface, two types of surfaces were examined using XPS; fractured (U3 and UCa3) and 0.5 μm diamond polished surfaces (UCa3, UCa2 and UCa1). The fractured surfaces were loaded into the XPS analysis chamber immediately, while the polished surfaces were exposed to air for a few hours before XPS analysis. Since the nominal U oxidation state in UCa3 is 5+, the amount of U^{6+} component at the surface is used to measure the degree of atmospheric oxidation. The XPS results show that the amount of surface oxidation is similar (~10% of total amount of U) for both the fractured and polished UCa3 surfaces, despite the fact that the polished surface was exposed to air for a longer period of time. This indicates that this sample is relatively stable towards surface oxidation after the initial exposure to air.

2.2. Spectroscopy

DRS spectra of the sintered pellet samples were collected at ambient temperature using a Cary 500 spectrophotometer equipped with a Labsphere Biconical Accessory, which utilises a beam spot size ~1 mm diameter. Spectra are converted into reflectance units by ratioing to the spectrum of a Labsphere certified standard (Spectralon), and then transformed into Kubelka–Munk units, $F(R) = (1-R)^2/2R$ [8]. At low sample concentrations and similar packing densities, we expect $F(R)$ to be proportional to the concentration of the material. Bandfitting was conducted using Bio-Rad Win-IR software.

XPS measurements were performed in ultra-high vacuum with a VG ESCALAB 220i-XL system employing a monochromatic AlK_α (1486.6 eV) X-ray source. The X-ray gun was operated at 120 W, and the spectrometer pass energy was set at 20 eV for regional scans. The diameter of the analysis area was approximately 500 μm, much larger than the average grain size. The thickness of the probed surface layer was approximately 5 nm. The specimens were mounted under a stainless steel foil with an open aperture of ~3 mm diameter. A low energy electron flood gun was used for the neutralisation of surface charge buildup in these insulating samples. The binding energies were calibrated by fixing the C 1s peak (due to adventitious carbon) at 285.0 eV. The surface concentration of different species was determined by integrating the peak area (after subtracting a Shirley-type background) with Scofield sensitivity factors as defined in the software package supplied by VG Scientific.

3. Results and discussion

The DRS spectra of U1, U2 and U3 are shown in Fig. 1, which also includes spectra of brannerite,

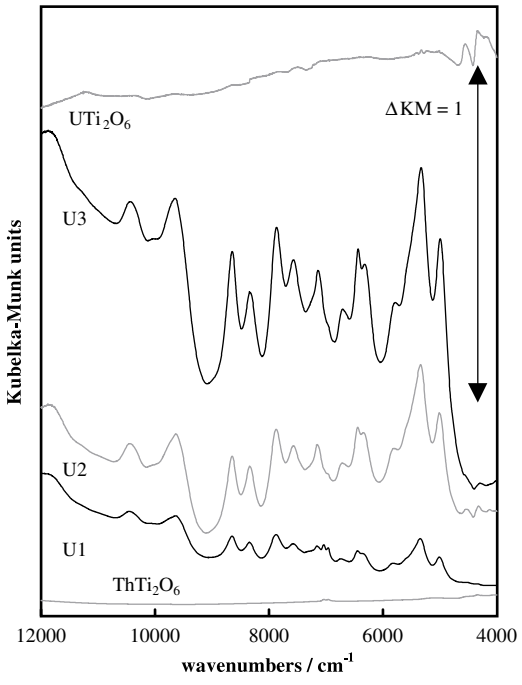

Fig. 1. DRS spectra (4000–12 000 cm^{-1}) of uranium doped in $ThTi_2O_6$; U1 ($Th_{0.97}U_{0.03}Ti_2O_6$), U2 ($Th_{0.9}U_{0.1}Ti_2O_6$), and U3 ($Th_{0.7}U_{0.3}Ti_2O_6$). The uppermost spectrum is of UTi_2O_6 (brannerite), and the lowest, of $ThTi_2O_6$ (thorutite).

UTi_2O_6, and thorutite, $ThTi_2O_6$. The spectra have been offset for clarity; reflectance values ranged between 0.8 and 0.2 for the doped $U_xTh_{1-x}Ti_2O_6$ samples ($F(R) \sim 0.03$–1.6 Kubelka–Munk units), and between 0.26 and 0.23 ($F(R) \sim 1.0$–1.3) in the case of brannerite. As discussed earlier, UTi_2O_6 shows virtually no spectral features over this wavelength range, although the low reflectance indicates that light is being heavily absorbed by the sample. Likewise, $ThTi_2O_6$ shows no spectral features, and in this case the high reflectance indicates that there is virtually no absorption in this region ($F(R) < 0.04$). In contrast, U1, U2 and U3 have a large number of weak bands ($\Delta F(R) < 1$) in the 5000–11 000 cm^{-1} region which increase in intensity with the U concentration, and are assigned to U^{4+}. By curve-fitting a small section of the spectrum (9000–7000 cm^{-1}), the integrated areas of the most accurately fitted band, at 7876 cm^{-1}, were calculated and found to vary in the ratio of 1:3.5:5.5, as compared to a nominal U ratio of 1:3.3:10. There are no notable band shifts or broadening occurring with increased U^{4+} concentration in the lattice, and thus the suggestion that electronic interaction could be resulting in loss of single-ion character [6] appears unlikely, at least over this concentration range. Instead, we propose that an increase in specular reflectance with increasing absorptance (i.e., due to increasing U^{4+} concentration), is responsible for the decreasing rates of growth of diffuse reflectance band intensities.

The DRS spectra of UCa1, UCa2 and UCa3 are shown in Fig. 2. Comparison with Fig. 1 reveals a number of new, prominent features in this region, including an intense, sharp doublet at ~6990 cm^{-1} (not resolved in UCa3) and three broader bands at 4550, 10 250 and 11 800 cm^{-1}. A higher lying broad band is observed at 14 000 cm^{-1} (not shown here). This is very similar to the spectrum obtained from air-fired U-doped zirconolite [14], which consists of a sharp band at 6650 cm^{-1}, and three broader bands at 9270, 10 720, and 13 400 cm^{-1}. Indeed, this pattern (with minor shifts) has been recognised as characteristic of U^{5+}, not only in the solid state, but in solution and the gas phase as well (cf. spectra of UCl_5) [5]. Assignment of these bands as due to U^{5+} is consistent with the presence of Ca^{2+} in the structure, which would be expected to force the oxidation of U as a charge-compensation mechanism (see above). The integrated areas of the sharp, and thus most accurately integrated U^{5+} band at 6990 cm^{-1} (summed where this appears as an unresolved doublet) varies as 1:3.2:4, compared to a nominal ratio of 1:3.3:10. However, in the case of UCa2, the band is already quite intense, with height ~1 KM units, and thus further threefold increase in concentration is not likely to be matched with a similar increase in band intensity.

In an octahedral bonding environment, the $^2F_{5/2}$ and $^2F_{7/2}$ components (split by spin–orbit coupling) of the U^{5+} ^2F electronic state are further split into 2 and 3

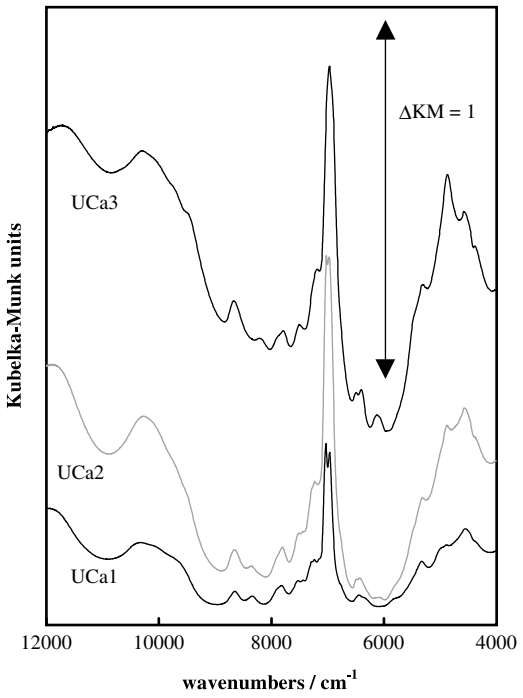

Fig. 2. DRS spectra (4000–12 000 cm^{-1}) of uranium and calcium doped in $ThTi_2O_6$; UCa1 ($Th_{0.955}U_{0.03}Ca_{0.015}Ti_2O_6$), UCa2 ($Th_{0.85}U_{0.1}Ca_{0.05}Ti_2O_6$) and UCa3 ($Th_{0.55}U_{0.3}Ca_{0.15}Ti_2O_6$).

levels, respectively. Further reduction in symmetry results in the ultimate splitting of these levels into 7 Kramers doublets as indicated in Fig. 3. The observed energy level structure is similar to that of other U^{5+} compounds such as $(NEt_4)UCl_6$, UCl_5 and $CsUF_6$ [5]. In contrast to U^{5+}, a much larger number of components (90) arise from the splitting of the ^3H, ^3F, ^3P, ^1G, ^1D and

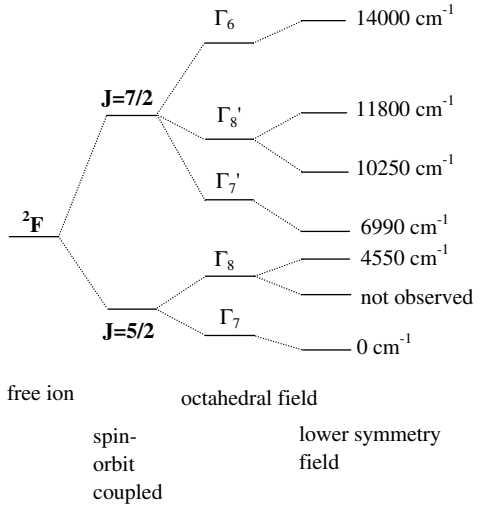

Fig. 3. Lowest electronic energy levels of U^{5+} in $ThTi_2O_6$.

^1I states of the f^2 configuration of U^{4+}, under spin–orbit coupling and ligand field effects. Extensive studies of U^{4+} in various lattices have been undertaken, requiring polarised measurements of single-crystals at low temperature (~4 K) for accurate assignments [5]. There is a complicating factor in the case of the DRS spectra, in that the splitting of the lowest $^3H_4$ multiplet can result in sufficiently low-lying energy states ($E < 500$ cm^{-1}) that significant populations at ambient temperature can occur. Thus we may expect to see some differences from the published low temperature spectra, even taking into account the reduction in resolution, resulting from the contribution from thermally populated states. To summarise, DRS spectra of U^{5+} are characterised by a small number of bands in the NIR, which are remarkably similar for different compounds. DRS spectra of U^{4+} and (lower oxidation states) are expected to consist of a much larger number of transitions throughout the NIR/visible region, and require characterisation for each crystal system of interest.

Although the probing depth of DRS is expected to be significantly greater than that of XPS, XPS results support the assignment of U^{4+} in $Th_{0.7}U_{0.3}Ti_2O_6$ (U3) and U^{5+} in $Th_{0.55}U_{0.3}Ca_{0.15}Ti_2O_6$ (UCa3). Fig. 4 shows the U 4f XPS spectra of the fractured U3 and UCa3 surfaces (the U3 spectrum has been offset for clarity). As seen, the U 4f peaks from UCa3 are located at higher (by about 1 eV) binding energies than those from U3, indicating a higher U oxidation state in UCa3. The shake-up satellite structure associated with the U 4f level is also very different between the two surfaces (the U $4f_{5/2}$ satellite peaks are marked as 'Sat.' in Fig. 4). The U3 surface has a satellite peak at about 7.1 eV higher binding energy than the main U $4f_{5/2}$ peak, while the UCa3 surface has a weaker satellite feature at roughly 8.3 eV higher binding energy. (Note that the position of the weak U $4f_{7/2}$ satellite peak in UCa3 cannot be determined accurately due to the overlap with the U $4f_{5/2}$ peak.) Our results are comparable to those observed by Bera et al. [13] in that the U^{4+} and U^{5+} $4f_{5/2}$ satellite peaks are located at about 6.8 and 8.5 eV, respectively, above the main peak.

The U 4f peak shape in Fig. 4 also indicates that there is more than one U species present at the surface of these samples. In order to separate the different components, the U $4f_{7/2}$ region was fitted with three mixed Gaussian/Lorentzian peaks (the spectra could not be fitted satisfactorily with fewer than three peaks). The peak position and width, as well as the ratio of the Gaussian and Lorentzian components (G/L), were all allowed to vary freely, but the width and the G/L ratio of the three peaks were set to be equal in each fit. The result of curve-fitting is shown in Fig. 5(a) and (b) (dashed line for each individual component and diamonds for the envelope of the fit). The resulting peak parameters are listed in Table 1, along with those reported from mixed uranium oxides with alkali and alkaline earth metals [13]. The peaks located at (379.9 ± 0.1), (381.0 ± 0.1) and (382.2 ± 0.1) eV are attributed to U^{4+}, U^{5+} and U^{6+}, respectively. The binding energy (BE) of U^{4+} is ~0.3 eV lower than those reported in [13] for alkali and alkaline earth uranates, and the BEs of U^{5+} and U^{6+} are approximately 0.2 and 0.5 eV higher, respectively, in our study (the intensity of the U^{6+} com-

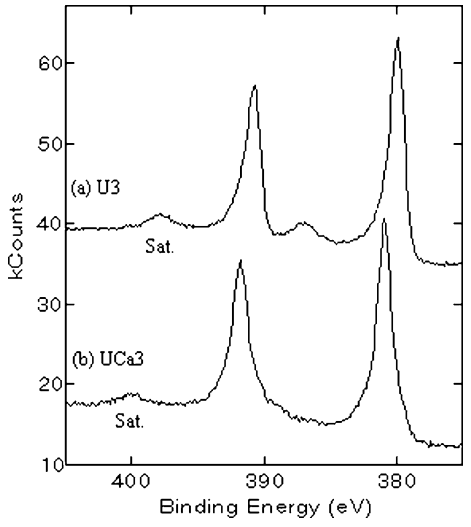

Fig. 4. U 4f XPS spectra of the fractured (a) U3 ($Th_{0.7}U_{0.3}Ti_2O_6$) and (b) UCa3 ($Th_{0.55}U_{0.3}Ca_{0.15}Ti_2O_6$) surfaces, with U $4f_{5/2}$ satellite peaks marked as 'Sat.'.

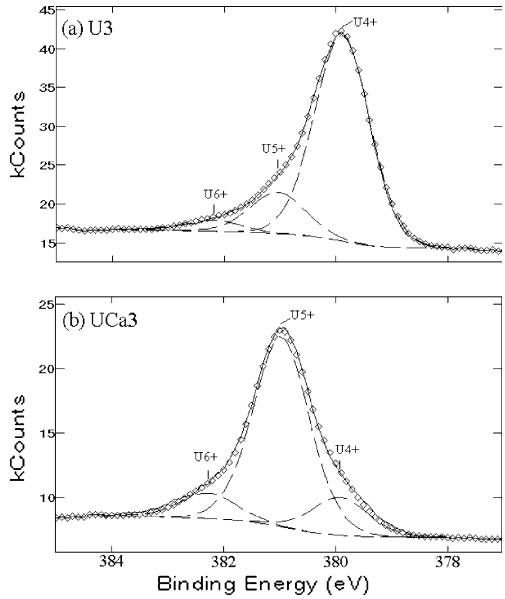

Fig. 5. Deconvolution of the U $4f_{7/2}$ photoelectron peaks from (a) U3 ($Th_{0.7}U_{0.3}Ti_2O_6$) and (b) UCa3 ($Th_{0.55}U_{0.3}Ca_{0.15}Ti_2O_6$).

Table 1
U $4f_{7/2}$ photoelectron peak parameters resulting from curve-fitting spectra of fractured $Th_{0.7}U_{0.3}Ti_2O_6$ (U3) and $Th_{0.55}U_{0.3}Ca_{0.15}Ti_2O_6$ (UCa3) surfaces, and those reported from mixed uranium oxides with alkali and alkaline earth metals [13]

		$Th_{0.7}U_{0.3}Ti_2O_6$ (U3)	$Th_{0.55}U_{0.3}Ca_{0.15}Ti_2O_6$ (UCa3)	Mixed U oxides [13]
U^{4+}	BE (FWHM), eV	379.9 (1.21)	379.9 (1.23)	380.2 (2.23)
	Intensity (%)	80	15	
U^{5+}	BE (FWHM), eV	381.0 (1.21)	381.0 (1.23)	380.8 (2.45)
	Intensity (%)	16	75	
U^{6+}	BE (FWHM), eV	382.2 (1.21)	382.3 (1.23)	381.7 (2.5)
	Intensity (%)	4	10	
G/L		0.28	0.39	

Note that the BEs from Ref. [13] are shifted by 0.4 eV as their calibration was based on fixing the C 1s peak at 284.6 eV.

ponent is much higher in [13] as the uranates contain U^{6+} in the bulk). One other notable difference is the much narrower photoelectron peaks from U3 and UCa3 (as indicated by the FWHMs in Table 1), mainly due to the monochromatic X-ray source employed in the current study.

As seen in Fig. 5(a) and (b), the dominant components in U3 and UCa3 are U^{4+} and U^{5+}, respectively. The small U^{5+} and U^{6+} components in U3 are believed to be the result of atmospheric oxidation at the surface, as is the U^{6+} component in UCa3. However, the presence of U^{4+} in UCa3 is not expected to be caused by vacuum reduction as these U/Ca-doped thorutite surfaces are quite stable under ultra-high vacuum. This is in agreement with DRS spectra showing residual U^{4+} bands in UCa3 (discussed below). The relative intensity of the U^{4+} peak seems to be dependent on the surface finish: the U $4f_{7/2}$ XPS spectrum of a polished UCa3 surface (not shown here) shows a larger U^{4+} component (~27% of total U amount). This increase in the U^{4+}/U_{total} ratio appears to be associated with the decrease in the amount of Ca^{2+} at the polished surface, which is approximately 60% of that on the fractured surface. As fractured ceramic surfaces are expected to contain more grain boundary areas than polished surfaces, this seems to suggest that Ca^{2+} is enriched along grain boundaries, leading to more oxidised U^{5+} species on the fractured surface. This is consistent with Ca^{2+} ions segregating to the grain boundaries during the high temperature sintering process.

Segregation of solutes in doped ceramics is a well-known phenomenon [15]. The ion mismatch provides a driving force for the segregation of Ca^{2+} in Ca/U-doped thorutite since the ionic radius of Ca^{2+} is larger than that of U^{4+}, U^{5+} and Th^{4+}. Substitution of Ca^{2+} on a Th^{4+}/U^{4+} site is expected to result in the formation of two U^{5+} ions to compensate the additional charge and hence the formula $Th_{(1-3x/2)}U_xCa_{x/2}Ti_2O_6$ should force the complete oxidation of U^{4+} to U^{5+}. However, due to enrichment of Ca^{2+} at grain boundaries, the amount of Ca^{2+} inside each grain would be less than the nominal amount, leading to incomplete conversion of U^{4+} to U^{5+}.

The residual U^{4+} component in the Ca-doped samples, noted in XPS data, is also evident in the superposition of the more prominent U^{4+} bands on the U^{5+} DRS spectra (Fig. 2). Comparison of the U^{4+} band intensities in U1 and UCa1 (Fig. 6) suggests that possibly as much as 50% of the U in UCa1 remains as U^{4+}. However, these bands appear with similar intensity in the UCa2 and UCa3 spectra (Fig. 2), although the total U concentration is considerably higher, so that the

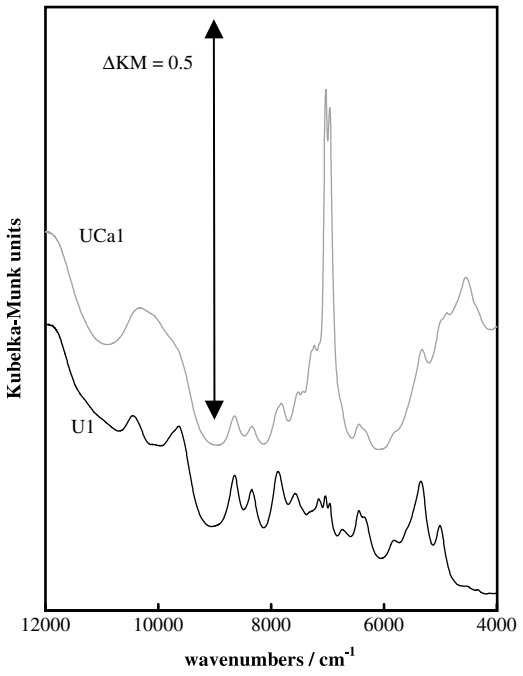

Fig. 6. DRS spectra (4000–12 000 cm^{-1}) of U1 ($Th_{0.97}U_{0.03}Ti_2O_6$) and UCa1 ($Th_{0.955}U_{0.03}Ca_{0.015}Ti_2O_6$), comparing the effect of adding Ca^{2+}.

proportion of residual U^{4+} in the most highly concentrated UCa3 is ~5%. The residual U^{4+} bands are also observed for an overdoped sample with composition $Th_{0.9}U_{0.05}Ca_{0.05}Ti_2O_6$, in which the amount of Ca^{2+} present is double that required to ensure complete oxidation of U^{4+} to U^{5+}. XPS analyses indicate that the relative amount of residual U^{4+} in the UCa series increases with decreasing concentration of (total) U. Based on the deconvolution of the U $4f_{7/2}$ XPS spectra of the polished UCa1, UCa2 and UCa3 surfaces (not shown here), the $U^{4+}/(U^{4+}+U^{5+})$ ratios are approximately 81%, 64% and 30%, respectively. For easy comparison, the U^{6+} component is neglected here, because the f^0 ion is not detectable using NIR spectroscopy. This trend is consistent with the segregation of Ca^{2+} in these materials, because the enrichment factor (defined as $C_{\text{grain boundary}}/C_{\text{bulk}}$) is expected to increase with decreasing solute concentration in the bulk [16].

It is interesting to compare the spectrum of U^{4+} in a different crystal lattice with that of brannerite. Fig. 7 shows the DRS spectra of 5.1 wt% U in perovskite (nominally $CaTiO_3$), compared with that of U2, 5.6 wt% U in thorutite (brannerite structure). Both XANES and XPS studies of the doped perovskite sample show that U is tetravalent in this system [17]. The space group of $CaTiO_3$ is D_{2h}^{16}, with U^{4+} occupying the Ca site, symmetry C_s, which lacks inversion symmetry. The U^{4+} bands are significantly more intense than in the corresponding brannerite structure, presumably due to the absence of an inversion centre for the U^{4+} site group symmetry in perovskite, thus allowing the formally parity-forbidden electric dipole transitions to some extent. The inversion centre in brannerite is lost with Ca^{2+} substitution (and thus formation of U^{5+}) and the lowered symmetry is likely to be a contributing factor to the intensity of the U^{5+} bands in the brannerite structure.

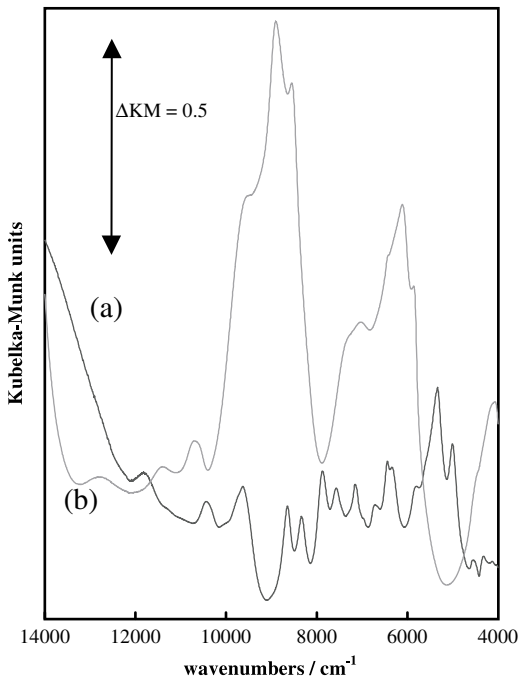

Fig. 7. DRS spectra (4000–14 000 cm^{-1}) of (a) 5.6 wt% U^{4+} in $ThTi_2O_6$ and (b) 5.1 wt% U^{4+} in perovskite.

4. Conclusions

NIR diffuse reflectance and X-ray photoelectron spectroscopies have been found to be useful means of deriving information about actinide speciation in nuclear waste forms; in this case, uranium in brannerite. The optical spectrum of U^{4+} has been identified in the brannerite structure by means of low concentrations of U^{4+} in the f^0 analogue, $U_xTh_{1-x}Ti_2O_6$, and consists of a large number of relatively weak bands throughout the NIR region, as expected on the basis of the predicted energy level structure of the f^2 ion. The addition of Ca^{2+} to substitute for U^{4+} in the lattice is charge-compensated predominantly by the oxidation of the uranium from U^{4+} to U^{5+}, enabling the measurement of the U^{5+} spectrum in this lattice, which consists of one relatively sharp and four broader NIR bands. Despite the lower probing depth than is the case for the DRS measurements, XPS analyses have confirmed the DRS results that U^{4+} is the dominant oxidation state in $Th_{0.7}U_{0.3}Ti_2O_6$, and U^{5+} in $Th_{0.55}U_{0.3}Ca_{0.15}Ti_2O_6$. However, weak U^{4+} bands were also observed by DRS in addition to the U^{5+} bands in all the Ca-doped materials, suggesting that a residual amount of U remains in the reduced state, even with the presence of excess Ca^{2+}. The appearance of U^{4+} in these materials could be explained by the actual Ca/U ratio inside each grain being lower than the nominal value (0.5) due to the segregation of Ca^{2+} to the grain boundaries during the sintering process. This is supported by XPS data, showing that contributions from U^{4+} were observed in all the Ca-doped samples, and that the concentration of residual U^{4+} increases with decreasing amount of Ca (and U) in the sample.

Evidence was found for decreasing rates (sublinear) of growth in DRS band intensities with U content >0.1 f.u. in thorutite (i.e., 5.6 wt% U in $ThTi_2O_6$). No spectral features attributable to U^{4+} were observed in the spectrum of UTi_2O_6, and this is considered to be due to the high concentration of U^{4+} in the lattice giving rise to increased specular reflectance in this sample. Comparison of the spectrum of 5.6 wt% U^{4+} in $ThTi_2O_6$ with that of a similar U^{4+} concentration in a perovskite lattice which lacks inversion symmetry at the U^{4+} site, indicates that loss of inversion symmetry is associated with increased band intensities, as expected for formally forbidden electric dipole transitions. In addition to stabilising the U^{5+} oxidation state, substitution with Ca^{2+}

also removes a local centre of inversion. Thus, the observed intensity of the U^{5+} transitions (relative to those of U^{4+}) in thorutite, is attributed to the loss of inversion symmetry with Ca^{2+} substitution.

Acknowledgements

The authors thank D. Attard and G. Smith for assistance with sample preparation, and Huijun Li for SEM analysis.

References

[1] A.E. Ringwood, S.E. Kesson, K.D. Reeve, D.M. Levins, E.J. Ramm, in: W. Lutze, R.C. Ewing (Eds.), Radioactive Waste Forms for the Future, Elsevier, Amsterdam, Netherlands, 1988, p. 233.
[2] B.B. Ebbinghaus, R.A. Van Konynenburg, F.J. Ryerson, E.R. Vance, M.W.A. Stewart, A. Jostsons, J.S. Allender, T. Rankin, J. Congdon, in: Waste Management '98 (CD-ROM; sess65/65-04), WM Symposia, Tucson, AZ, USA, 1998.
[3] E.R. Vance, M.L. Carter, B.D. Begg, R.A. Day, S.H.F. Leung, in: R.W. Smith, D. Shoesmith (Eds.), Scientific Basis for Nuclear Waste Management XXIII, Materials Research Society, Pittsburgh, PA, 2000, p. 431.
[4] B.D. Begg, E.R. Vance, S.D. Conradson, J. Alloys Compounds 271/273 (1998) 221.
[5] W.T. Carnall, H.M. Crosswhite, in: J.J. Katz, G.T. Seaborg, L.R. Morss (Eds.), The Chemistry of the Actinide Elements, 2nd Ed., vol. 2, Chapman & Hall, London, 1986 (Chapter 16).
[6] E.R. Vance, J.N. Watson, M.L. Carter, R.A. Day, G.R. Lumpkin, K.P. Hart, Y. Zhang, P.J. McGlinn, M.W.A. Stewart, D.J. Cassidy, Ceram. Trans., Am. Ceram. Soc. 107 (2000) 561.
[7] E.R. Vance, J.N. Watson, M.L. Carter, R.A. Day, B.D. Begg, J. Am Ceram. Soc. 84 (1) (2001) 141.
[8] G. Kortüm, Reflectance Spectroscopy, Springer-Verlag, Berlin, 1969.
[9] R.K. Vincent, G.R. Hunt, Appl. Opt. 7 (1968) 53.
[10] B.W. Veal, D.J. Lam, in: Gmelin Handbook of Inorganic Chemistry, Springer, Berlin, 1982, p. 176 (Supplement, vol. A5).
[11] D. Chadwick, Chem. Phys. Lett. 21 (1973) 291.
[12] G.C. Allen, J.A. Crofts, M.T. Curtis, P.M. Tucker, D. Chadwick, P.J. Hampson, J. Chem. Soc. Dalton Trans. (1974) 1296.
[13] S. Bera, S.K. Sali, S. Sampath, S.V. Narasimhan, V. Venugopal, J. Nucl. Mater. 255 (1998) 26.
[14] E.R. Vance, G.R. Lumpkin, M.L. Carter, D.J. Cassidy, C.J. Ball, R.A. Day, B.D. Begg, J. Am. Ceram. Soc. 85 (2002) 1859.
[15] J. Nowotny, in: J. Nowotny (Ed.), Science of Ceramic Interfaces, Elsevier, Amsterdam, Netherlands, 1991, p. 79.
[16] G.S.A.M. Theunissen, A.J.A. Winnubst, A.J. Burggraaf, J. Mater. Sci. 27 (1992) 5057.
[17] E.R. Vance, M.L. Carter, Z. Zhang, K.S. Finnie, B.D. Begg, in preparation.